1 Shape Optimization of a Photo Gun

1.1 Geometry

- initial geometry in Figure 1
- corresponding electric field for $p = 3$, $n_{\text{sub}} = 16$, $V_{\text{el}} = -300$ kV and $V_{\text{ar}} = 1$ kV

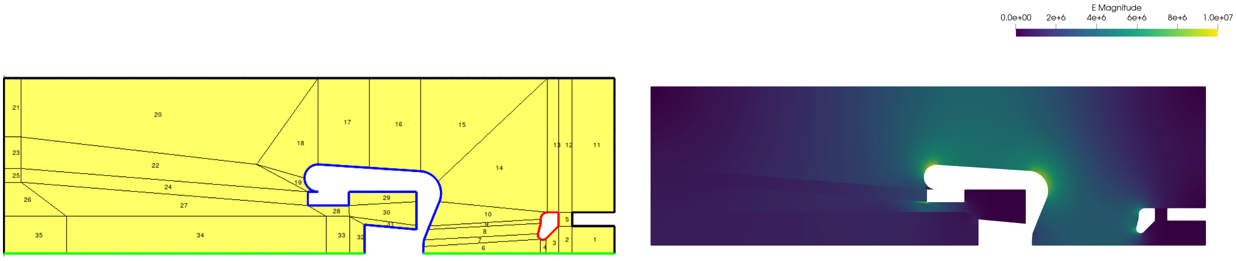

Figure 1: Initial geometry and magnitude of electric field.

1.2 Optimization

- optimized geometry in Figure 2
- corresponding electric field for $p = 3$, $n_{\text{sub}} = 16$, $V_{\text{el}} = -300$ kV and $V_{\text{ar}} = 1$ kV
- cost function employs $I = \{14, \dots, 19\}$
- **results**:

	$(V_{\text{el}} - 625)$ in cm^3	$\frac{1}{\lvert I \rvert} \sum_{i \in I} \max_{\mathbf{x} \in \Omega_i} \lVert \mathbf{E}(\mathbf{x}) \rVert_2$ in $\frac{\text{MV}}{\text{m}}$	$\max_{\mathbf{x} \in \Omega} \lVert \mathbf{E}(\mathbf{x}) \rVert_2$ in $\frac{\text{MV}}{\text{m}}$
initial	2.458	7.858	9.272
optimized	-55.532	6.625	7.318

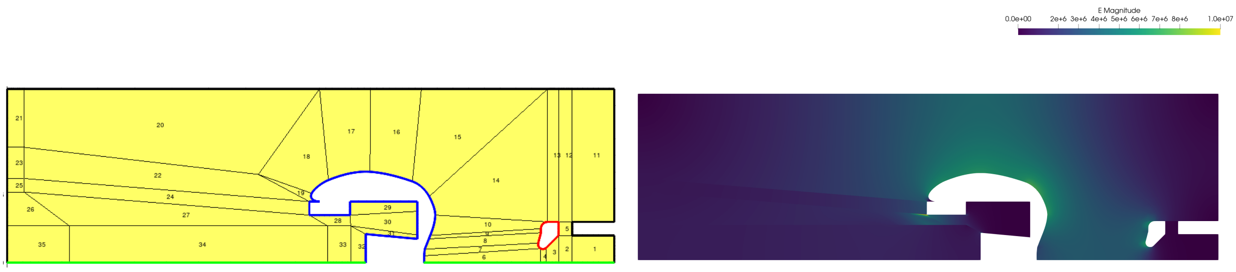

Figure 2: Optimized geometry and electric field.

1.3 Tracking

- **general settings**: $Q = 100$ fC
- **spatial distribution**: see Figure 3 for distribution generated from measurement and for comparison with laser measurement
- see Figure 4 for spatial distribution from Gaussian ($\sigma = 400\ \mu$m)
- **temporal distribution**: Gaussian with $\sigma = 5$ ps (is measurement data available?)

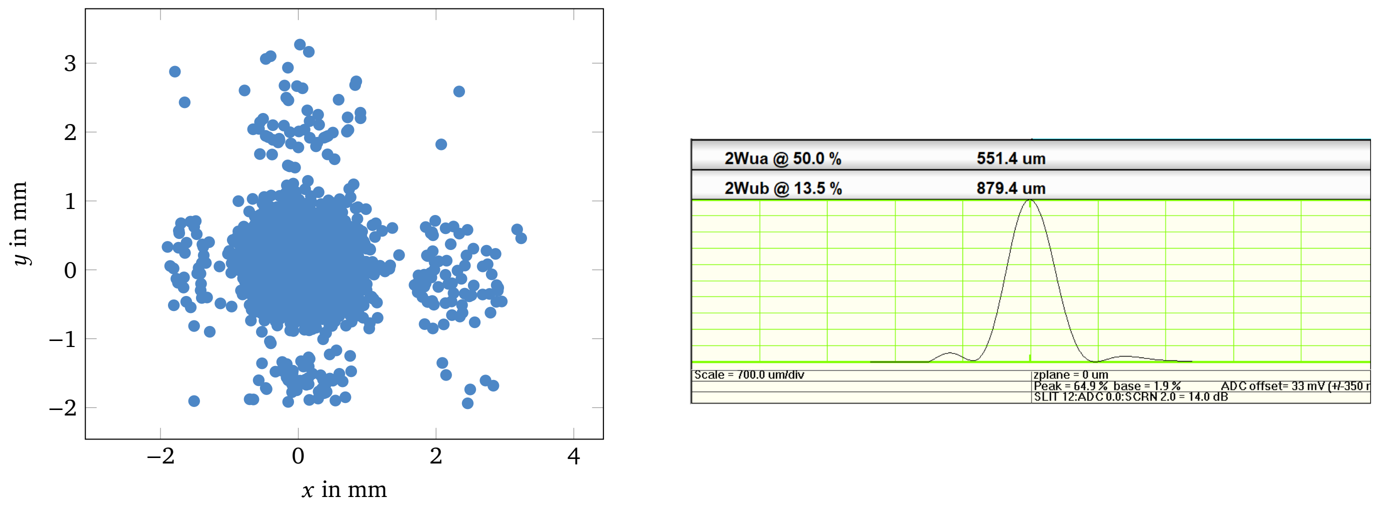

Figure 3: Spatial distribution generated from measurement (2^{11} particles) and laser measurement.

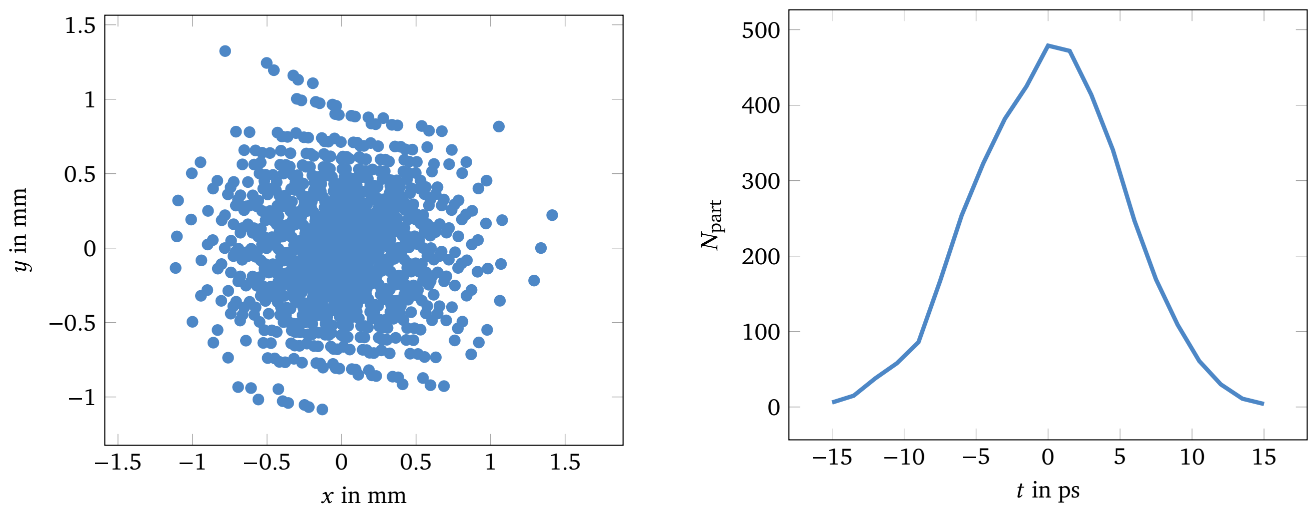

Figure 4: Spatial distribution from Gaussian ($\sigma = 400\ \mu$m, 2^{10} particles) and temporal distribution (2^{11} particles).

- **convergence of time integrator**: relative error of normalized transverse emmitance ϵ w. r. t. finest time step is shown in Figure 5
- computed with $n_x = n_y = 8$ ($h_x = h_y = 1.875 \cdot 10^{-4}$) and $n_z = 256$ ($h_z = 4.258 \cdot 10^{-4}$)
- $H = 2^{-12}$ ns used later on

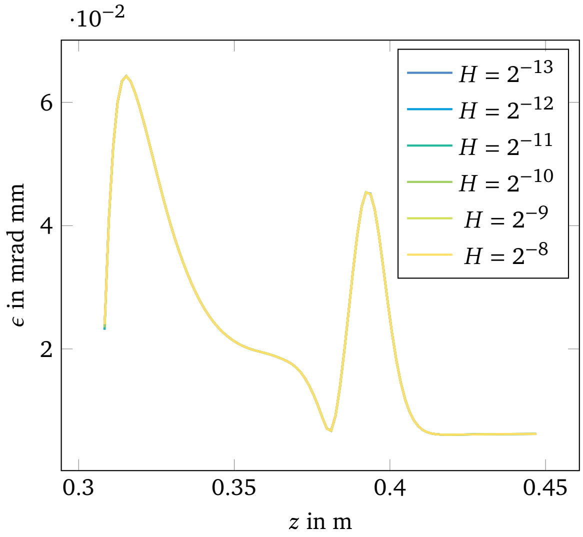

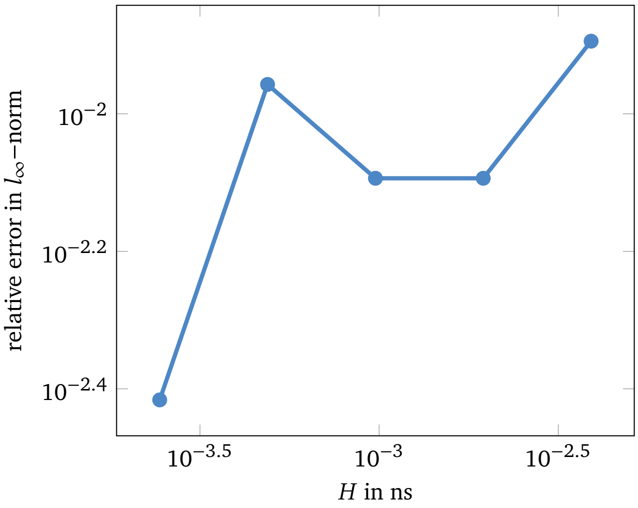

Figure 5: Normalized transverse emmitance and relative error in l_∞-norm.

- **convergence of field map**: look at convergence with number of grid points in transverse (n_x, n_y) and longitudinal (n_z) direction individually
- Figure 6 looks at convergence of n_x, n_y for $n_z = 64$ ($h_z = 1.703 \cdot 10^{-3}$)
- Figure 7 looks at convergence of n_z for $n_x = n_y = 8$ ($h_x = h_y = 1.875 \cdot 10^{-4}$)
- $n_x = n_y = 8$ ($h_x = h_y = 1.875 \cdot 10^{-4}$) and $n_z = 256$ ($h_z = 4.258 \cdot 10^{-4}$) used for convergence studies later on
- $n_x = n_y = 16$ ($h_x = h_y = 2.5 \cdot 10^{-4}$) and $n_z = 256$ ($h_z = 4.258 \cdot 10^{-4}$) used for simulation later on (distribution from measurement is larger then that from Gaussian by more then a factor 2, see Figure 3 and Figure 4)

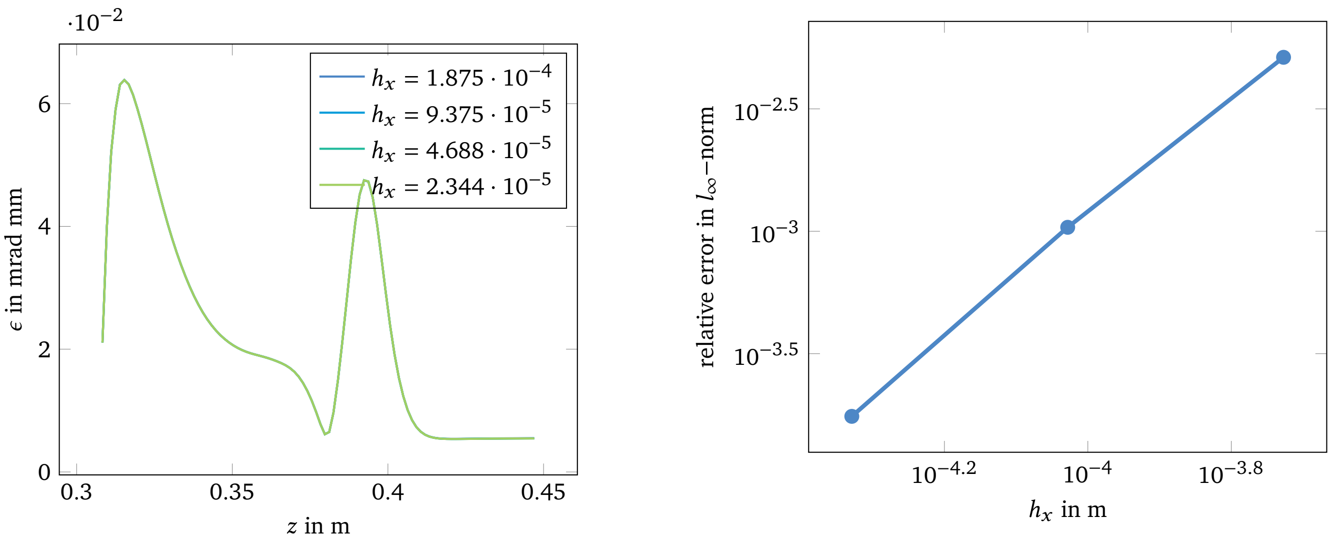

Figure 6: Normalized transverse emmitance and relative error in l_∞-norm for $n_z = 64$ ($h_z = 1.703 \cdot 10^{-3}$) and $n_x = n_y$ variable.

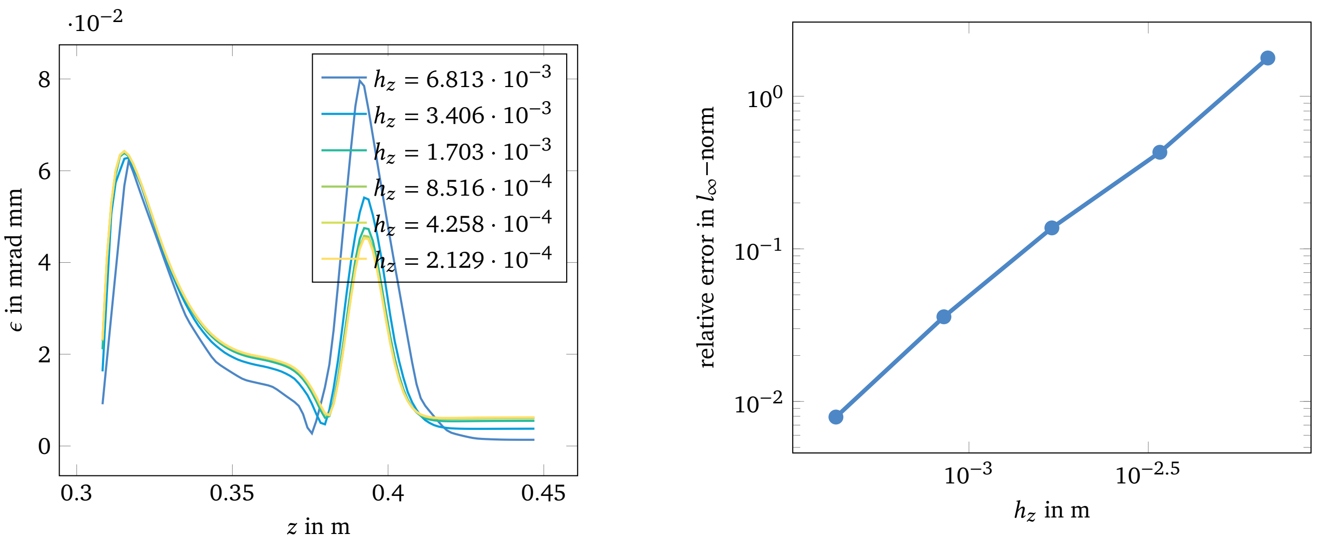

Figure 7: Normalized transverse emmitance and relative error in l_∞-norm for n_z variable and $n_x = n_y = 8$ ($h_x = h_y = 1.875 \cdot 10^{-4}$).

- **convergence of space charge**: look at convergence with number of grid cells in radial (n_r) and longitudinal (n_l) direction and number of particles (n_I) separately
- Figure 8 looks at convergence of n_r, n_l for $n_I = 2^{10}$
- $n_r = n_l = 64$ ($h_r = 2.344 \cdot 10^{-5}, h_l = 1.703 \cdot 10^{-3}$) used later on
- Figure 9 looks at convergence of n_I for $n_r = n_l = 64$ ($h_r = 2.344 \cdot 10^{-5}, h_l = 1.703 \cdot 10^{-3}$)
- $n_I = 2^{11}$ used for simulation later on

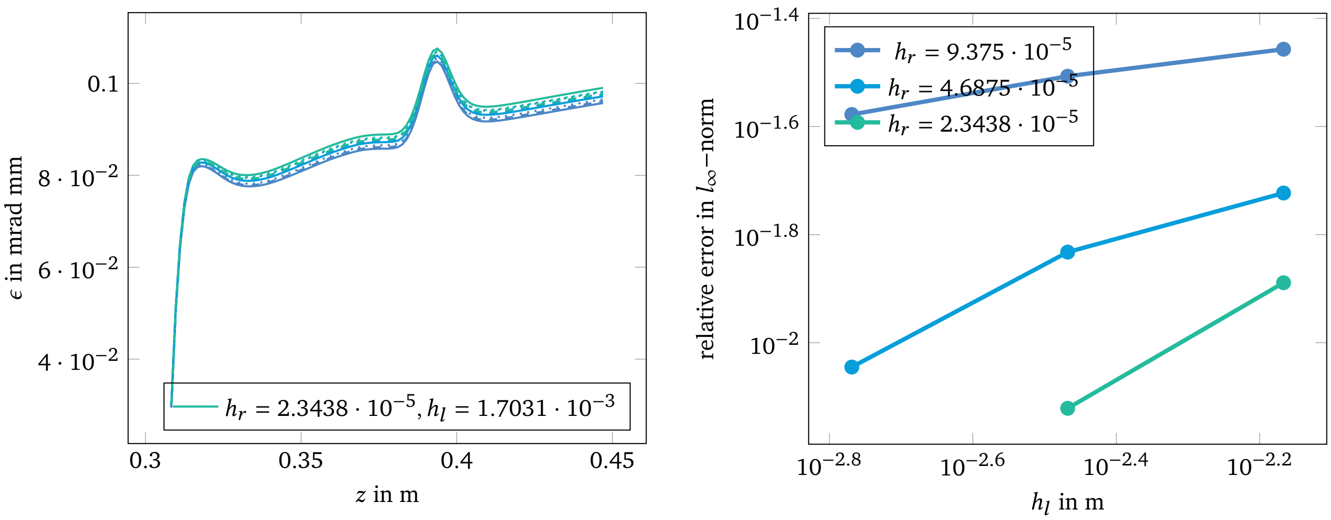

Figure 8: Normalized transverse emmitance and relative error in l_∞-norm for $n_I = 2^{10}$ and n_l, n_r variable.

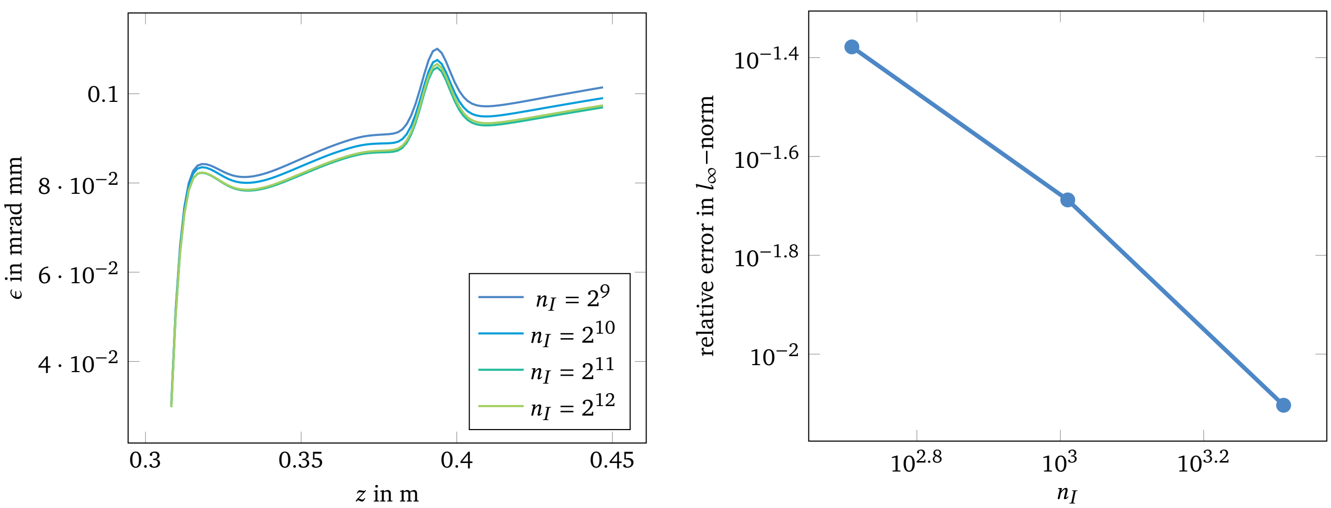

Figure 9: Normalized transverse emmitance and relative error in l_∞-norm for n_I variable and $n_r = n_l = 64$ ($h_r = 2.344 \cdot 10^{-5}, h_l = 1.703 \cdot 10^{-3}$).

- **tracking results**: simulation results for initial and optimized geometry
- continued tracking for 15 cm into the beam pipe
- initial normalized transverse emmitance for $H = 2^{-12}$, $n_x = n_y = 8$, $n_z = 256$, $n_r = n_l = 64$, $n_I = 2^{11}$ and refined ($H = 2^{-13}$, $n_x = n_y = 16$, $n_z = 512$, $n_r = n_l = 128$, $n_I = 2^{12}$) in Figure 10 (uses Gaussian distribution, $\tilde{\epsilon}$ signifies refined solution)
- optimized normalized transverse emmitance for $H = 2^{-12}$, $n_x = n_y = 16$, $n_z = 256$, $n_r = n_l = 64$, $n_I = 2^{11}$ also in Figure 10 (uses distribution from measurement)
- rms beam size of initial geometry in Figure 11
- rms beam size of optimized geometry in Figure 12
- **results**:

	relative error of ϵ in l_∞−norm	relative error of x_{rms} in l_∞−norm
x	$3.38 \cdot 10^{-3}$	$6.046 \cdot 10^{-3}$
y	$4.277 \cdot 10^{-3}$	$1.027 \cdot 10^{-2}$

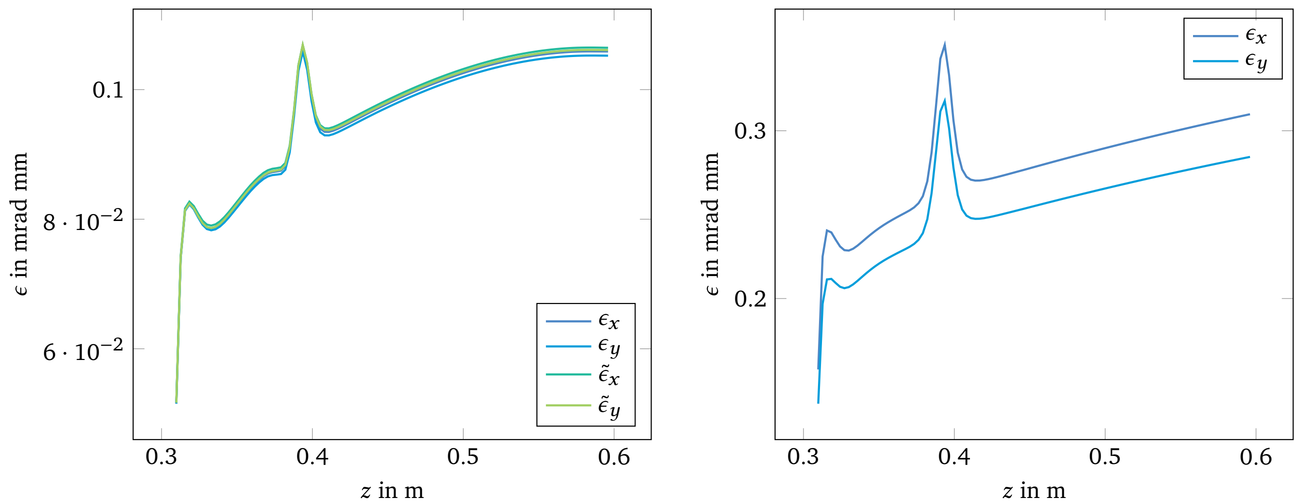

Figure 10: Normalized transverse emmitance of initial and optimized geometry.

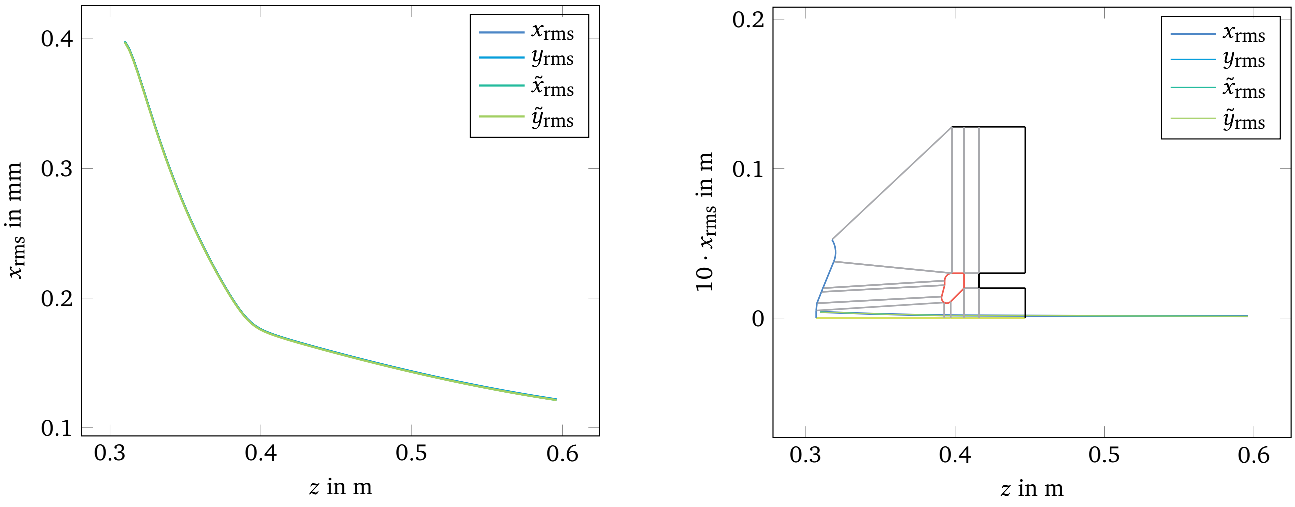

Figure 11: RMS beam size of initial geometry.

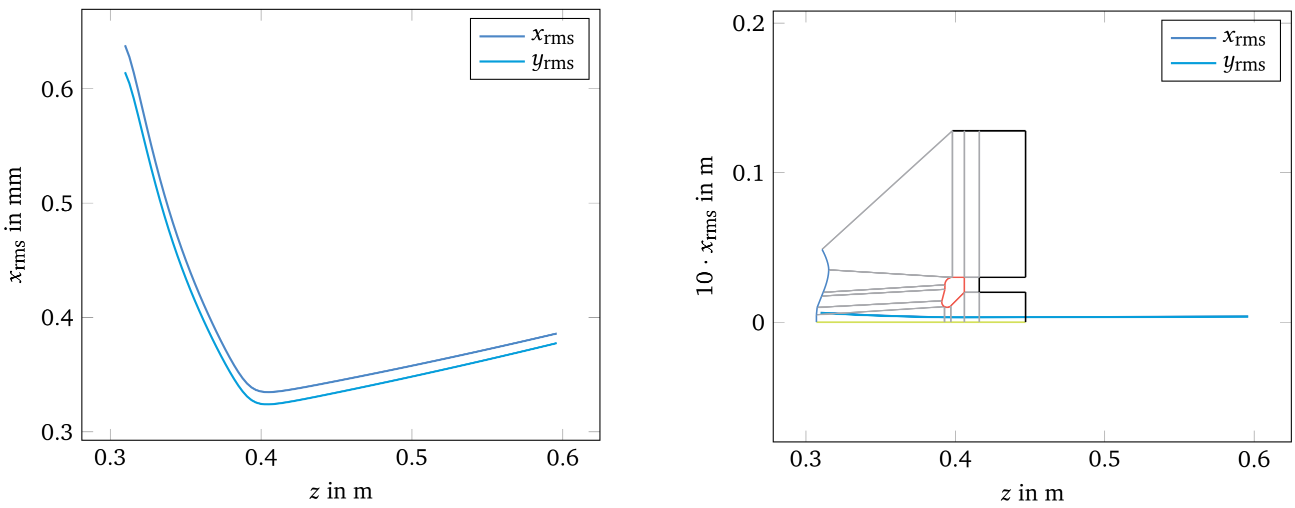

Figure 12: RMS beam size of optimized geometry.

References

[1] Markus Wagner. "Production and investigation of pulsed electron beams at the S-DALINAC". PhD thesis. Technische Universität Darmstadt, 2013.